JOURNAL OF SPACECRAFT AND ROCKETS
Vol. 37, No. 3, May–June 2000

Oxygen Interaction with Materials III: Data Interpretation via Computer Simulation

Jean-François Roussel* and Alex Bourdon†
ONERA, 31055 Toulouse, France

The Evaluation of Oxygen Interaction with Materials III experiment, flown by NASA on STS-46, allowed the characterization of the Space Shuttle local environment and the products of material erosion by atomic oxygen (AO) by mass spectrometry. Relatively complex transport mechanisms were involved in that environment, namely, gas-phase collisions and wall reflections. Several situations were simulated by a numerical model: quiescent period or thruster operation, orientation of spectrometer to analyze Shuttle environment or erosion products, and materials directly exposed to ram flux or covered by a baffle. The comparison between numerical and experimental results yielded good agreement. That contributed to the experiment interpretation and the validation of the model. It pushed model parameters toward a large AO accommodation and a small Kapton® erosion efficiency at low AO energy.

Nomenclature

E	= kinetic energy of impinging atomic oxygen (AO), eV
k	= Boltzmann constant, $J \cdot K^{-1}$
m	= molecule or atom mass, kg
n	= number of molecules of CO resulting from the erosion of one monomer of Kapton® by AO
n_{ambient}	= density of natural ambient environment, m^{-3}
n_{thermal}	= density of species at thermal velocity in Shuttle frame (outgassed molecules and AO after reflections), m^{-3}
R	= equivalent radius of Shuttle in a simple analytical model, m
R_1, R_2	= rate of Kapton erosion by AO, cm^3/atom
S_r	= ratio of random to average velocity in Maxwellian distribution of reflected molecules in Nocilla[13] model (~Mach number)
V_r	= average velocity of reflected molecules in Nocilla[13] model, m/s
v_{ambient}	= velocity of drifting ambient natural molecules in Shuttle frame, m/s
$v_{\text{outgassed}}$	= average velocity of outgassed molecules, typically hundreds of meters per second, m/s
α, α_1, α_2, α_3	= accommodation coefficient
θ_i	= angle of incident molecule velocity to surface normal, rad
θ_r	= angle of reflected molecule velocity to surface normal, rad
λ_{ambient}	= mean free path for self-scatter of ambient molecules (natural atmosphere), m
$\lambda_{\text{ambient-thermal}}$	= mean free path of natural ambient molecules due to collisions with thermalized species, m
$\lambda_{\text{outgassed-ambient}}$	= mean free path of outgassed molecules due to collisions with the natural ambient environment, m
σ	= elastic collision cross section, m^2
$\phi_{\text{outgassed}}$	= flux of outgassed molecules, molecule $\cdot m^2 \cdot s^1$
ϕ_{return}	= return flux of outgassed molecules into Shuttle bay, molecule $\cdot m^2 \cdot s^1$

Received 12 April 1999; revision received 25 January 2000; accepted for publication 27 January 2000.

*Research Scientist, Département Environnement Spatial, Centre d'Etudes et de Recherches de Toulouse.

†Ph.D. Student, Département Environnement Spatial, Centre d'Etudes et de Recherches de Toulouse.

Introduction

THE Evaluation of Oxygen Interaction with Materials III (EOIM-III) flight experiment,[1–3] flown on STS-46 in 1992, produced a large amount of data, essentially in the form of mass spectra. It covered the characterization of the Space Shuttle general environment in quiescent periods and during thruster operations, as well as the very local environment of materials eroded by atomic oxygen (AO).

In many situations, the observed molecular species had to undergo a complex transport mechanism to reach the mass spectrometer. Such is the case, for instance, for thruster effluent backflow into Shuttle bay or for AO, which proved to be able to pass around a cover to reach a priori protected materials. A good analysis tool for molecular transport is numerical modeling (contrarily to contaminant production or effects, which are primarily taken from experiment). The present study consisted in the modeling of the EOIM-III environment, either limited to the Shuttle bay or with a larger extension around Shuttle. The aim pursued was twofold: first, to help experimental data interpretation and, second, to validate the numerical model.

The experimental devices and results are summarized in a first section. Then the numerical simulations and their results are presented and compared to experimental data. Three successive cases are considered: the backscatter of outgassed molecules, the backflow of thruster effluents in the Shuttle bay, and eventually the detailed dynamics in the bay.

Experiment

A detailed description of the experiment, mass spectrometer calibration, and preliminary analysis of the results has already been published by the designers of the experiment.[1–3] Only information necessary for the comparison to modeling results, therefore, is provided here. The experimental data during thruster firings are as yet unpublished.

Experimental Device

The EOIM-III mass spectrometer was mounted on a rotating device that allowed operation in two different orientations. In the so-called tilt-up orientation (first part of Fig. 1), the spectrometer was pointed out of the Shuttle bay, which was the ram direction during (almost) all of the EOIM experiment. The bay-to-ram attitude of Shuttle was aimed at maximizing AO fluence. The AO flux and the Shuttle local environment were characterized in that orientation. The tilt-down orientation, also shown in Fig. 1, allowed the detection of the products of the erosion of the materials covering the five sectors of the carousel. The five materials were ^{13}C-labeled Kapton®, anodized aluminum, Chemglaze Z306 black paint, FEP Teflon®, and Parylene-C. However, most of the erosion products of these materials were already present in the local induced atmosphere of Shuttle,

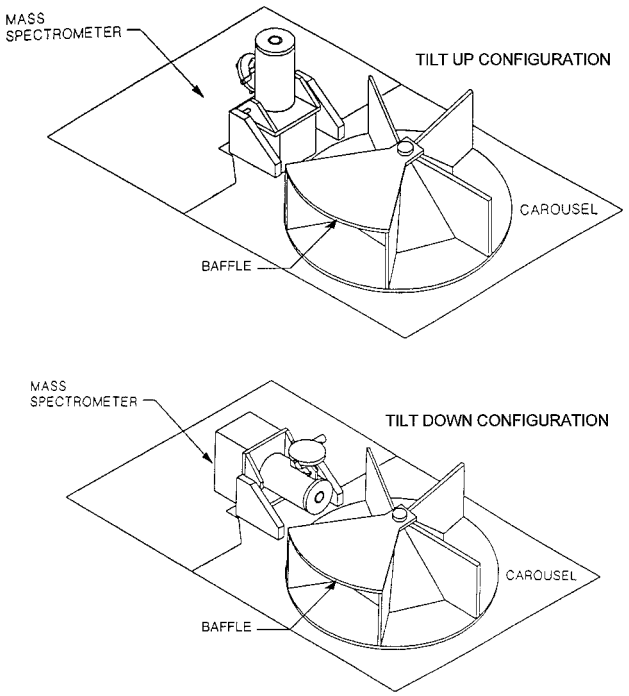

Fig. 1 Mass spectrometer and carousel in tilt-up position for ambient atmosphere measurements (mass spectrometer faces ram direction) and tilt-down position for measurements of erosion products.

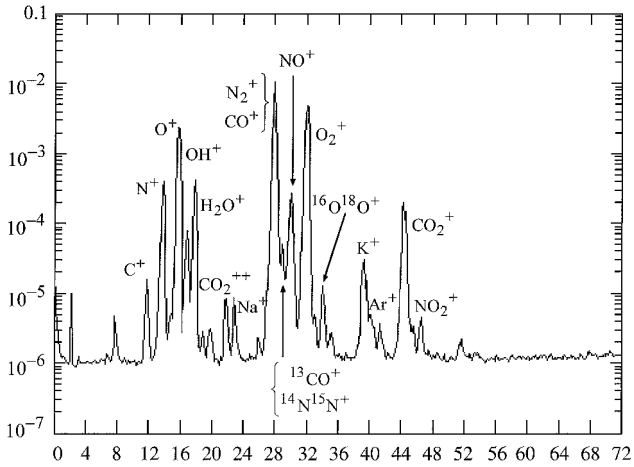

Fig. 2 Typical mass spectrum of ambient environment in tilt-up position.

and only the ^{13}C-labeled Kapton turned out to be really suitable for quantitative measurements because of the labeled carbonated products ^{13}CO and $^{13}CO_2$. A baffle could also be moved above the sector facing the spectrometer, prohibiting the direct impingement of AO onto the considered material. It can be seen over another sector of carousel in Fig. 1. Calibration of the mass spectrometer was first performed on the ground at the Los Alamos National Laboratory (LANL),[3] but the decay of sensitivity was different in-flight, and a new in-flight calibration was necessary.[1]

Overview of Experimental Data

Three typical spectra taken at the beginning of the EOIM-III experiment, at 231-km altitude, are shown in Figs. 2–4. The first one, in tilt-up position, shows, as is well known, that the Shuttle local ambient environment is not only composed of natural species (O, N_2, O_2, and Ar), but also of species emitted by the Shuttle (H_2O, CO, and CO_2) or resulting from gas-phase or surface reactions (NO, NO_2, etc.). Human contamination is also visible (Na and K), and most other species are the result of cracking in the spectrometer ionization chamber.

The spectrum of Fig. 3 shows the species coming from the Kapton sector, not covered by the baffle, measured in tilt-down position.

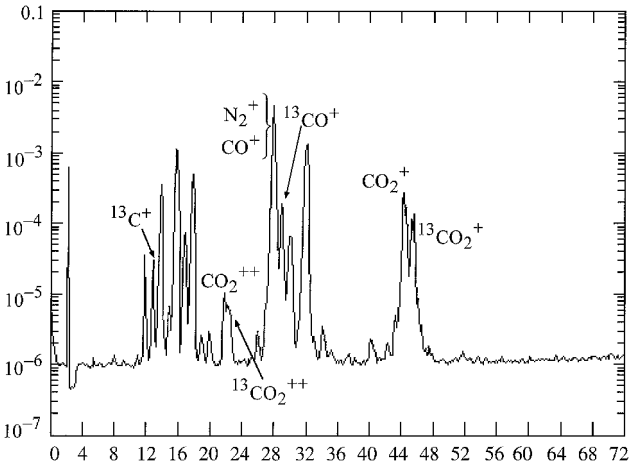

Fig. 3 Typical mass spectrum in tilt-down position facing Kapton coated sector, without baffle.

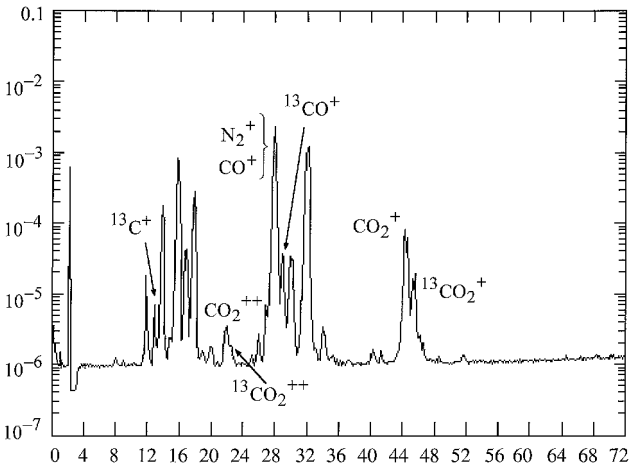

Fig. 4 Typical mass spectrum in tilt-down position facing Kapton, with baffle.

Most of the species are similar to the preceding spectrum, with a decrease by a factor close to 2, which simply shows that the species of the local environment can bounce on Kapton and reach the spectrometer. New mass peaks are, however, present, denoting the emission of ^{13}C-labeled molecules ^{13}CO and $^{13}CO_2$ due to AO erosion.

The Kapton used in that experiment contained approximately 50% of ^{13}C and 50% of ^{12}C. Thus, it is not surprising to see a peak of $^{12}CO_2$ a little larger than the peak of $^{13}CO_2$, because ambient $^{12}CO_2$ adds to the first peak. A crude quantitative computation can already be attempted at that level. It follows from the equal quantity of ^{12}C and ^{13}C originating from Kapton erosion that the contribution of ambient CO_2 must be the difference between mass 44 and mass 45, that is, approximately $2 \times 10^{-4} - 1 \times 10^{-4} = 1 \times 10^{-4}$ μA, concerning peak maximum. Considering the maximum of 2×10^{-4} μA of ambient CO_2 visible on the preceding tilt-up spectrum (Fig. 2), this value is consistent with the approximate general reduction of peak heights by a factor 2 between tilt-up and tilt-down spectra, due to bounces.

The most striking feature of the next spectrum (Fig. 4), with the baffle covering the observed Kapton sector, is its similarity with the preceding one, without baffle. The species are identical, and most current intensities are almost unaffected by the presence of the baffle. In fact, the peaks of ambient species (O, H_2O, N_2, NO, O_2, and CO_2) are almost unchanged, whereas the products of erosion (^{13}CO and $^{13}CO_2$) are approximately reduced by a factor of 5.

The absence of signal decrease for the molecules of the ambient environment shows that they can pass around the baffle. The carousel and spectrometer have effectively been designed in such a way that the 2π-sr view of the spectrometer was almost completely covered by the carousel sector facing it and the baffle. Moreover, gas-phase collisions in spectrometer field of view cannot be invoked because the mean free path is always at a minimum tens of meters, even in case of the largest ram pressure increase. Hence,

the ambient molecules observed, including AO, really go under the baffle, certainly due to bounces on walls of the bay and mass spectrometer support. However, AO seems to have a reduced eroding power. Simulations reported subsequently will show that all of this is consistent with bounces and AO energy reduction resulting in a lower erosion efficiency.

Another major concern to contamination scientists is constituted by thruster effluents. Although only the lightest and, thus, the most volatile of them could be measured by the EOIM spectrometer, the study of their flux into Shuttle bay is very interesting because it involves complex transport mechanisms, namely, wall reflections and gas-phase collisions, which also are of concern with heavier, more condensable effluents. Comparison to the modeling of that process in next section will be particularly profitable because the major contribution of such models is in the transport model, the outgassing or thruster emitted fluxes being taken from experiment.

An example of a Vernier reaction control system (VRCS) firing is shown in Fig. 5. The grid current of the spectrometer ionization chamber is representative of the total pressure. That current increases to 3×10^{-3} μA during the period 662,535–662,554 s mission elapsed time (MET), whereas it is quite constant at 2×10^{-3} μA during quiescent periods. Contrary to the too short operating periods of the primary reaction control system (PRCS), this 18-s VRCS firing is long enough for several spectra to be acquired during thruster operation inasmuch as the 72 masses are swept within 5.12 s. The first and second spectra of Fig. 5, before and during the thruster firing, respectively, are represented in detail in Figs. 6 and 7. Several of the thruster effluents can be identified. The water peak increases significantly while new peaks appear: mass 46 is NO_2, and masses 26 and 27 are almost certainly CN and HCN but could also be C_2H_2 and C_2H_3, although no mass 25 revealing C_2H is ever visible. Other species, such as CO, N_2, NO, and CO_2, are masked by the high level of the ambient environment for those masses. Others, such as OH, are also due to cracking in the ionization chamber.

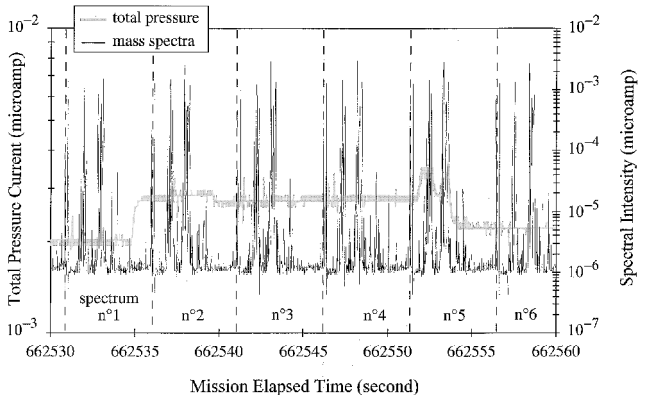

Fig. 5 Total pressure and spectra over a period including an operation of VRCS R5D thruster.

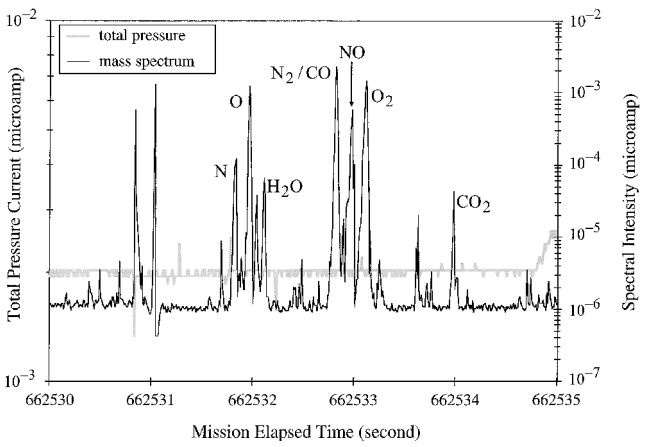

Fig. 6 First spectrum of Fig. 5: before thruster firing.

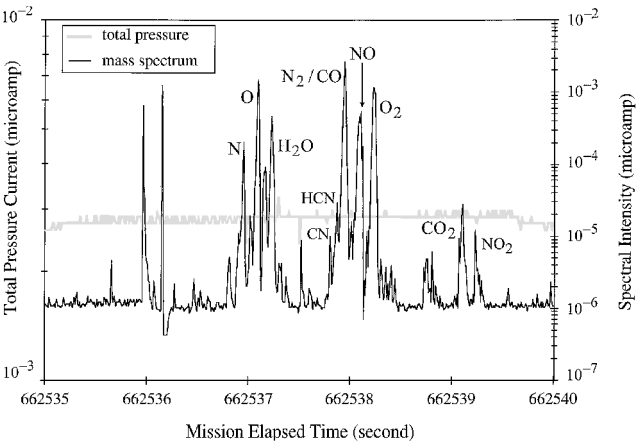

Fig. 7 Second spectrum of Fig. 5: during thruster operation.

Modeling and Comparison to Experiment

Shuttle External Environment in Quiescent Periods

The first situation that was modeled is the induced environment around the Shuttle in quiescent periods, that is, in the absence of thruster firing or any other operation. It is certainly the simulation in which the possible comparison to experiment is expected to be the crudest. Although the natural environment (O, N_2, etc.) is correctly known due to EOIM measurements in tilt-up position, the sources of species contributing to the induced environment, essentially outgassing, are not known accurately. In particular, outgassing fluxes depend on the temperature of the surfaces at the time considered but also earlier in the mission. Because these data were not available, simple average data for Shuttle outgassing after one week in space were used. A total outgassing rate of 10^{19} molecule $\cdot m^{-2} \cdot s^{-1}$ was assumed, composed of 60% of water, 20% of N_2 and 20% of CO_2 molecules. It was assumed to be homogeneous, although tiles, for example, are known to outgas, more water than other surfaces. The time interval studied was MET 554,000–554,600 s, during which tilt-up measurements were performed. The natural environment was determined directly from EOIM experimental data, which for AO gave a flux of 5.0×10^{19} m^{-2} s^{-1}, and thus a density of 6.2×10^{15} m^{-3}, which amounts to assuming that the natural atmosphere reaches the spectrometer almost unperturbed.

Such ambient densities yield typical mean free paths for outgassed molecules through collisions with the natural ambient environment of the order of

$$\lambda_{\text{outgassed-ambient}} = (1/\sigma n_{\text{ambient}}) \times (v_{\text{outgassed}}/v_{\text{ambient}}) \sim 100 \text{ m} \quad (1)$$

Collisions are, thus, a second-order phenomenon that cannot be neglected yet because Shuttle typical dimensions are tens of meters. Hence the Boltzmann equation is to be solved. This was done with the particle method direct simulation Monte Carlo (DSMC) using Bird's time counter method.[4,5] The computation box was about 100 m in each of the three directions. It was considered sufficient to extend it to several times the Shuttle size rather than several times the mean free path because the outgassed molecules that encounter their first collision farther than 100 m from Shuttle, although numerous, have little chance to return to the Shuttle because of the small solid angle it covers, when seen from that distance.

The DSMC model[6] was included in the more general code for simulation of local environment and contamination of spacecraft[7] (SILECS). Figure 8, where the AO density is represented in a median fictitious plane, also gives an idea of the Shuttle surface meshing. The ram AO density increase is by a factor 5 at maximum (ram flux is downward in Fig. 5). The depleted wake, also visible, extends more behind the wings than the fuselage because of their larger breadth.

The main purpose of that modeling, however, was the comparison of quantitative results of the numerical simulation to experimental data, namely, to fluxes into the bay, measured in the tilt-up position. The results are summarized in Table 1, where the return fluxes of the three outgassed species (H_2O, CO_2, and N_2) are given.

Table 1 Fluxes of outgassed molecules backscattered into Shuttle bay

Species	Experiment return flux[a]	Numerical simulation: Return flux[a]	Numerical simulation: Outgassed flux[a]	Numerical simulation: Return flux ratio, %	Analytical return flux ratio, %
H_2O	0.23	0.47	6.0	7.8	4.6
N_2	?	0.18	2.0	9.1	5.7
CO_2	0.25	0.23	2.0	11.8	7.1

[a]Fluxes $\times 10^{18}$ $m^{-2} \cdot s^{-1}$.

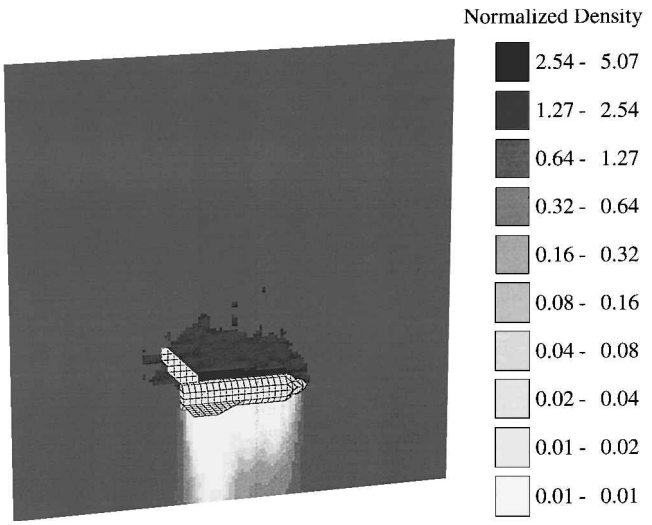

Fig. 8 AO density (ambient flux is going down).

The return flux of outgassed N_2 could not be determined in the experiment because it is a major constituent of the natural environment. The agreement between the experiment and simulation return fluxes for H_2O and CO_2 (first two columns of Table 1) is within a factor 2, which is satisfactory, considering uncertainties in outgassed fluxes. These values were obtained as a result of calibration factors measured on the ground[8] for thermal H_2O and CO_2. In a previous publication by the present authors,[6] these calibration data were not known to the authors and a high-velocity AO calibration factor[1,3] was used for H_2O and CO_2, which led to important discrepancies with numerical results.

The fourth column of Table 1 also gives the ratio of backflow flux to outgassed flux. The values of the order of 10% are quite high but typical of the very low altitudes (230 km) and relatively high densities ($\sim 5 \times 10^{15}$ m^{-3}) of the EOIM-III mission. Table 1 indicates that the heavier the molecules are, the larger the return ratio is. From one molecule to the other, three factors change, which could explain that: the cross section, the molecular mass and its consequences on kinematics, and the emission velocity. The major factor turns out to be the third one, the velocity, which is slower for heavier molecules emitted with thermal distribution from the same surface (at 300 K in the present simulations). This results in a longer stay in the vicinity of the Shuttle, where an impingement by AO can lead to a return to the Shuttle. The cross sections used [variable hard sphere[5] (VHS)] for collisions of AO with H_2O, N_2, or CO_2 are all in the range 13–15 $Å^2$ at orbital velocity, which excludes the first factor. The second one, that is, kinematics, also seems to be of little effect because the high velocity of AO guarantees a velocity oriented backward after one collision even for the heavy CO_2 molecules.

The last two columns of Table 1 compare the numerical predictions of backflow ratio with those of a simple analytical model.[9] Approximation of the Shuttle as a sphere gives the following value for return flux:

$$\phi_{\text{return}} = \phi_{\text{outgassed}}(R/\lambda_{\text{ambient}})(v_{\text{ambient}}/v_{\text{outgassed}} + 1) \qquad (2)$$

where the sphere radius $R = 2.4$ m is often used.[9] The variation of the return ratio for the three outgassed species is similar to the numerical simulation. As in the simulations, it is due to the outgassed species velocity, as it is can be seen in Eq. (2). The absolute values of the return ratio are smaller, but this is certainly due to the crude approximation of the Shuttle as a sphere. A larger radius R, more representative of the Shuttle breadth, especially around the rear of the bay (taking the wings into account), could of course give quasi-identical values.

Note that the assumption that the natural unperturbed atmosphere (O, N_2, etc.) was correctly measured by the spectrometer was checked a posteriori. Natural species could effectively be perturbed by a too dense Shuttle-induced environment and only reach the spectrometer after many collisions, if ever. The mean free path for collisions of natural ambient molecules with molecules (quasi) thermalized in Shuttle frame (outgassed species and AO after bounces) of density n_{thermal} is

$$\lambda_{\text{ambient-thermal}} = 1/\sigma n_{\text{thermal}} \sim 300 \text{ m} \qquad (3)$$

for n_{thermal} of the order of several 10^{16} molecule $\cdot m^{-3}$, which was obtained in simulations in the nearest proximity to the Shuttle. Moreover, because this mean free path rapidly increases with distance to Shuttle, it could be expected that few of the ambient molecules were deviated by collisions before reaching the spectrometer. Eventually it was checked in simulations that about 94% of them reached the Shuttle bay without scattering.

Shuttle External Environment During Thruster Firings

The Shuttle environment was then modeled during the R5D VRCS operation reported earlier. At that time, AO density was 5.0×10^{15} m^{-3}. The VRCS plume was described by Simons's model (see Ref. 10), that is, an analytical fit of experimental fluxes on plume freezing surface. The total mass flow rate was simplified to 13.6 g/s of H_2O, 18 g/s of molecules of mass 28 atomic mass unit (amu) (CO and N_2 together), and 1.67 g/s of CO_2. No thruster exhaust quantitative data were found about the traces of mass 26 and 27 (certainly CN and HCN) detected experimentally; thus, they could not be included in the model.

The density of water stemming from thruster is shown in Fig. 9 in the symmetry plane of the simulation. The ambient flux still comes downward in Fig. 9 because the EOIM attitude is bay to ram. The relatively important density of thruster effluents above the Shuttle, while the R5D thrust direction is downward, is simply explained by the reflections of some molecules on the Shuttle wing, which intercepts the external part of the plume. Reflected molecules can then be backscattered into the bay by ambient atmosphere, which explains why thruster firing in the opposite direction can be detected by a pressure increase in the bay.

The experimental fluxes into the bay (tilt-up measurements) just before thruster ignition and during thruster operation are presented in Table 2. The difference is interpreted as the extra flux coming from

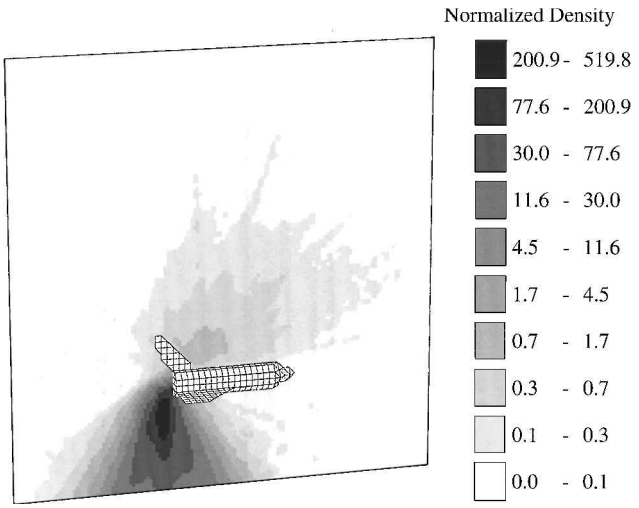

Fig. 9 Density of water effluent from R5D VRCS. (Ambient flux is going down.)

Table 2 Fluxes of thruster effluents reaching Shuttle bay

	Experiment				
	Averaged intensity, nA				
Species	Before thruster firing	During thruster firing	Difference	Return flux[a]	Simulation return flux[a]
H_2O	0.6	5	4.4	0.44	0.45
N_2/CO	27	30	3	1.6	0.42
CO_2	0.28	0.41	0.13	0.023	0.023
O	13	15.5	2.5	——	——

[a]Fluxes $\times 10^{18}$ $m^{-2} \cdot s^{-1}$.

thruster and is compared to the modeling results (last two columns). The agreement is very good concerning H_2O and CO_2 backflow. This accuracy is of course only the consequence of chance because the uncertainties of those computations are quite high and could crudely be estimated to a factor 2. [A very approximate assessment could be 10% from Monte Carlo statistical fluctuations, 30% for reflection and collision modeling, 20% for ambient flux measurements, and perhaps more due to the simple Simons's model (see Ref. 10) of the thruster plume.]

That was the main achievement of that simulation. The case of mass 28 (CO and N_2) shown in Table 2, for which, however, there seems to be a large discrepancy between computed and measured backflows, can also be studied. Note that the experimental signal increase during thruster operation is of the order of 10% for N_2/CO, whereas it is about 700% and 50% for H_2O and CO_2. Thus, the difference is much more subject to errors and could simply be discarded as not significant. However, the discrepancy with the model result can certainly be understood and is thought to be an artifact due to a variation of the calibration factor with velocity. To understand that, a small parenthesis about velocity influence on calibration factor is in order.

The calibration factors relating signal to flux were measured on the ground[3,8] in a range of velocity of 3–6 km/s, and the calibration factor for AO was found to be independent of velocity and equal to $(3.6 \pm 1) \times 10^{23}$ (atoms cm^{-2} s^{-1})/A. However, the large uncertainty of this calibration, associated with the small range of velocity tested, does not guarantee that there is no velocity effect at all. Moreover, two arguments are in favor of an increased calibration factor at smaller velocity. First, calibration factors relating a flux to a detector signal are only constant in theory for closed ionization sources, whereas they depend linearly on velocity for perfect open sources[11] (fly-through), in which signal is in fact proportional to density rather than flux. The ionization source of the EOIM-III mass spectrometer is of an intermediate semi-open type,[3] which should, thus, exhibit some dependence on velocity, but not as important as a linear dependence. The second argument comes from the calibrations that, for one species, namely, argon, were performed both at thermal velocity[8] and at high velocity[3,8] showing that the calibration factor was about seven times larger at thermal velocity than at orbital velocity.[11] (The analysis of Ref. 11 requires a translation of the density-to-signal calibration factor given in Ref. 8 for thermal species into a flux-to-signal calibration factor such as the ones given for high-velocity species in Refs. 3 and 8.) The variation is not as large as the velocity change, which is about a factor 50, but the variation seems to prove some velocity influence.

Thus, assuming some increase of spectrometer sensitivity at reduced incident velocity, the 11% increase of N_2/CO signal during thruster operation can be interpreted as being partly due to the velocity loss of some of the natural ambient N_2 molecules through collisions with thruster exhaust. The increase due to backflow is, therefore, drastically reduced. This effect can also be enhanced by direction changes because most scattered N_2 molecules are no longer directed along the spectrometer entrance axis. Moreover, that is confirmed by a similar increase of AO signal by 19% (fourth row of Table 2), which cannot presumably be explained by anything other than a sensitivity increase. It is not surprising that the effect is larger for AO than for N_2 because the velocity loss for the lighter AO through scattering is larger. A more quantitative interpretation is attempted in Ref. 11.

A specific study of $O + N_2$ collisions was performed in Ref. 12 and provides interesting insights. First, it confirms the validity of the total elastic cross section used here (2.0×10^{-20} m^2 here at 8 km/s relative velocity and 1.8×10^{20} m^2 in Ref. 12 for the corresponding energy in center-of-mass kinetic energy, 3.5 eV). Then, the differential cross section for $O + N_2$ inelastic collisions shows that energy losses due to such reactive collisions are important (half of the losses are due to elastic scattering) even though the integrated inelastic cross section is a decade smaller. The same effect certainly happens for backscattering because the differential inelastic cross section favors backscattering when compared to the isotropic hard sphere differential cross section (in center-of-mass frame). However, this effect does not seem sufficient to explain the observed discrepancy, which is as large as a factor of 4.

Shuttle Bay Environment

Modeling

Understanding the experimental spectra obtained in tilt-down position, when the spectrometer faced baffled or unbaffled carousel sectors, required detailed modeling of the experiment and of the inside of the Shuttle bay. The fluxes into the bay, measured in tilt-up position, were taken as input to these simulations.

The dynamics of molecules and atoms in the bay is dominated by reflections on the walls. The mean free path, although sometimes reduced to tens of meters, remains large enough for particles to encounter at least 10 times more reflections than collisions. In particular, concerning the experimental observation that particles could pass around the baffle, reported earlier, gas-phase collisions showed negligible effects when compared to bounces.

Thus, modeling of reflections was treated as carefully as possible, using the lobular model introduced by Nocilla[13] with recent experimental parameters.[14] The Nocilla[13] model is intermediate between purely specular or diffuse reflection models. For one direction and one energy of impinging molecules or atoms, the distribution of velocities after bouncing is assumed to be Maxwellian with an average velocity V_r and (pseudo) Mach number $S_r = V_r/(2kT_r/m)^{1/2}$. The central velocity V_r is described by its angle θ_r to surface normal and the classical accommodation coefficient α for its norm. From the several studies reviewed in Ref. 14, some of them concerning AO on various materials, the following values were extracted for Nocilla[13] model parameters:

$$S_r = 0.4 + 0.7\theta_i, \qquad \theta_r = 1.41\theta_i, \qquad \alpha = \begin{cases} \alpha_1 = 0.8\cos(0.8\theta_i) \\ \alpha_2 = 0.9\cos(0.4\theta_i) \\ \alpha_3 = 0.95 \end{cases} \tag{4}$$

where S_r is of the order of 1, and is even smaller around normal incidence, which means a rather diffusive model. Three different values were tested for α; the smaller α_1 corresponds to an average of values of Ref. 14, and the larger α_3 is certainly more representative of reflections on reactive materials or polymers. Other studies of AO diffusion[15] and accommodation[16] by inorganic materials (metals, glass, anodized aluminum) confirmed that these reflections are rather diffusive and accommodative, but gave no data specific to Kapton. Accommodation coefficients of about 0.6 were measured[16] on inorganic materials and should by higher on the more reactive Kapton.

Material erosion by AO was also modeled. It was limited to Kapton because quantitative measurements were only available for ^{13}C-labeled Kapton. The global Kapton erosion rate by 5 eV AO is about 3.1×10^{-24} cm^3/atom. It is known to produce essentially light species. Because heavy species were not measured, Kapton erosion was assumed to follow the reaction

$$C_{22}H_{10}O_5N_2 + (46\text{-}n)O \rightarrow 5\,H_2O + 2\,NO + n\,CO + (22\text{-}n)CO_2 \tag{5}$$

where the ratios of oxidation products are determined by stoichiometry, except for $[CO_2]/[CO]$, which was left open with parameter n. A ground Kapton erosion experiment[17] indicated $n \sim 2$, that is, $[CO_2]/[CO] \sim 10$, but EOIM flight data rather favor $[CO_2] \sim [CO]$. Only the sum $[CO_2] + [CO]$ shall be considered here.

Table 3 Ratios of AO fluxes between different spectrometer-carousel configurations

		Simulation accommodation coefficient		
Ratio considered	Experiment	α_1	α_2	α_3
Tilt down/tilt up	0.39	0.47	0.47	0.49
Baffle on/baffle off	0.86	0.66	0.66	0.71

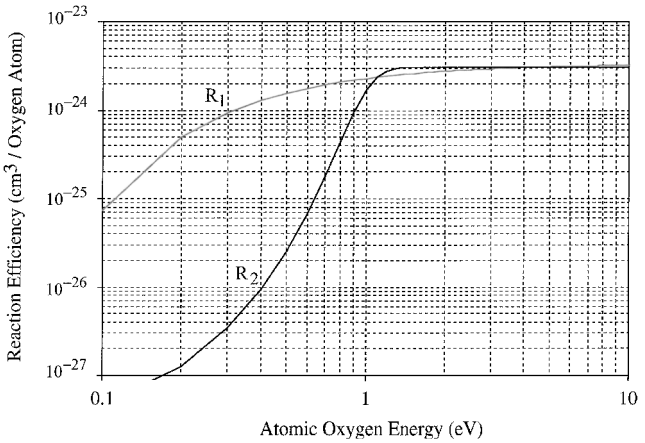

Fig. 10 R_1 and R_2 rates for Kapton erosion by AO.

At smaller impinging energies, Kapton erosion is not so well characterized, and two different laws for energy dependence were found in the literature:

$$R_1[E(\text{eV})] = R_1(5\,\text{eV})e^{-0.38/E} \tag{6}$$

in Ref. 18, and the Beckerle–Ceyer model

$$R_2[E(\text{eV})] = \frac{R_2(5\,\text{eV})}{1 + e^{-10(E-0.98)}} \tag{7}$$

in Ref. 2. Although both formulas are based on experiments at high and low energy, they differ significantly at small energy, as shown in Fig. 10.

The products of erosion were assumed to be emitted at thermal energy (300 K). This assumption has no effect on the fluxes, at least as long as no collisions are involved.

Results

The carousel-spectrometer apparatus was operated in three different configurations, tilt-up orientation, tilt-down orientation without baffle on the observed sector, and tilt-down orientation with baffle (see Fig. 1). Only the tilt-up orientation of spectrometer was relevant to the study of backflow into the bay discussed in preceding sections. The modeling of molecular dynamics in the bay now allows the prediction of experimental tilt-down data.

The existence of several different configurations is an opportunity to circumvent calibration issues by considering ratios of the same mass peak between these configurations. Although not discussed here, absolute measurements are a very delicate matter, and the EOIM spectrometer calibration certainly suffers from relatively large uncertainties. For example, the predicted AO sensitivity decay[3] (a factor 3.8 over the whole mission) was to be corrected after the flight[1] (to a factor 5.7). Moreover, the sensitivity decay is unknown for species such as CO_2, and, thus, the decay law of AO should be used. However, ground measurements indicated that the decays for Ar and O were different[3] (a factor 5.2 and 3.8 over mission time, respectively), and effectively, a detailed study of flight data[11] seems to indicate a faster sensitivity decay for CO_2 than for O.

The dynamics of AO are examined first. The AO density in the Shuttle bay is represented in Fig. 11. The ram pressure increase in the bay is due to random AO trajectories "trying to" exit from that cavity, but also due to AO deceleration or accommodation. By the following of the preceding idea, AO fluxes into the spectrometer are given as ratios in Table 3, first tilt-down (without baffle) over tilt-up fluxes, and then baffle on over baffle off (both tilt down of course).

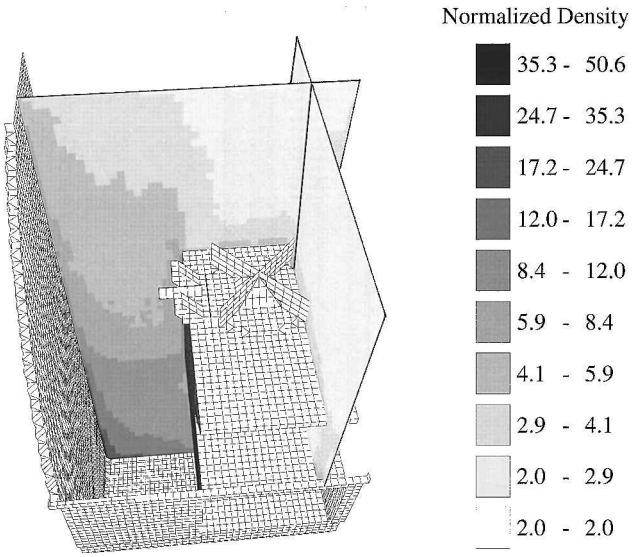

Fig. 11 AO density in Shuttle bay (accommodation coefficient α_1).

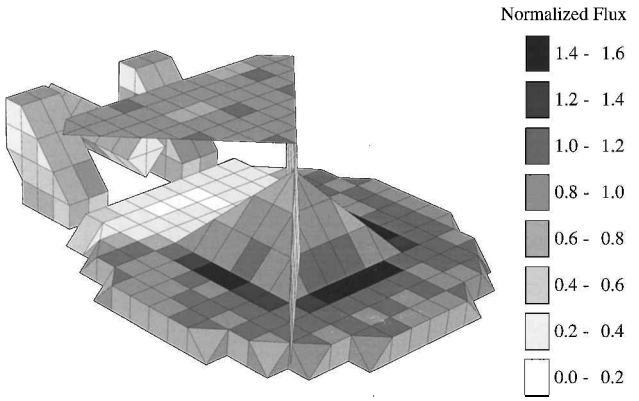

Fig. 12 AO flux onto carousel sectors with baffle on. (A dividing wall was removed to visualize the sector covered by the baffle.)

The results of the simulation compare favorably to the experimental data. This essentially checks the laws of AO diffusion by reflections. The AO fluxes are independent of the accommodation coefficient α used (up to statistical fluctuations), which was expected, because α only governs the norms of velocities, whereas orientations are controlled by S_r and θ_r (unchanged here). The tilt-down/tilt-up ratio, about 0.4 due to AO diffusion, is not surprising. On the contrary, the baffle-on/baffle-off ratio, relatively close to 1, which was already discussed when first looking at the spectra, was judged more surprising. However, it is correctly reproduced by simulations, which shows that AO can simply pass around the baffle due to bounces on the walls of the bay or of the experiment. Another enhancement factor for AO baffle-on flux is that most of the atoms that go under the baffle come out in the direction of spectrometer, whereas they can directly leave the bay in the absence of the baffle. However, the real experimental ratio could be somewhat smaller because the sensitivity of spectrometer could be higher for the slower oxygen atoms of the baffle-off configuration because they undergo more bounces than in the baffle-on configuration (cf. the discussion on calibration factor variation with energy in the section on thruster firing). The computed AO fluxes under the baffle and on the other sectors of the carousel can be seen in Fig. 12. Figure 12 shows that the AO flux onto the baffled sector is reduced by a factor of the order of 0.3. This reduction factor is smaller than the one of the spectrometer AO signal due to the baffle (~0.7 in simulations, cf. Table 3) because AO coming back from under the baffle is also preferentially direct toward the instrument as just discussed. Flux enhancement around concave edges of unbaffled sectors is due to reflected oxygen atoms.

The last results to be discussed are the fluxes of erosion products. Table 4 gives the ratios of fluxes of carbonated erosion products

Table 4 Tilt-down/tilt-up ratios of fluxes of Kapton erosion products, for two erosion rates and three accommodation coefficients compared to experiment

Kapton erosion rate	Experiment	Simulation accommodation coefficient		
		α_1	α_2	α_3
R_1	0.14	0.55	0.45	0.29
R_2	0.14	0.57	0.39	0.24

(computed from $^{13}CO_2$ + ^{13}CO signals) in the presence and in the absence of a baffle. The experimental ratio, 0.14, is rather small and shows that although an important amount of AO could pass around the baffle, AO has lost some of its eroding capability, certainly because of energy loss in reflections. The mechanism is easy to understand. Oxygen atoms reaching Kapton have undergone more reflections if they had to pass around the baffle; hence, they have lost more energy because of accommodation, and finally they erode less Kapton because the erosion rate is smaller at low energy.

Thus, it is not surprising that, in the simulations, higher accommodation, α_2 and α_3, or smaller erosion efficiency, R_2, at low AO energy yield a smaller ratio. The average kinetic energy of AO reaching Kapton for α_1 is substantially reduced from 4.8 and 3.6 eV (respectively, without and with baffle) to 3.3 and 1.1 eV when α_3 is used in the simulation. Although the ratios computed by the simulations for three different accommodation coefficients, α_1, α_2, and α_3, and two reaction rates, R_1 and R_2, are in general significantly larger than 0.14, the case with the largest accommodation, α_3, and smallest erosion efficiency, R_2 at low AO energy gives an approaching ratio 0.24.

Thus, it can be concluded that numerical simulations favor a large accommodation coefficient and a small erosion efficiency at low energy for AO. These parameters certainly constituted the most reasonable assumptions: Accommodation is known to be quite large on reactive polymers and α_1 was certainly too low; R_2 smaller erosion rate at low energy[2] may also be thought to be more reliable than the older R_1 rate.[18]

A last remark can be done about absolute values of $^{13}CO_2$ and ^{13}CO fluxes, although relative values, that is, ratios, were preferably studied here until now. Whereas absolute fluxes of AO are correct (thanks to in-flight recalibration), absolute fluxes of carbonated erosion products are about a factor of 5 larger in the simulation than in the experiment, when using the AO sensitivity decay law. Because uncertainties on erosion rates and molecular dynamics are much lower than that, that discrepancy is certainly due to a different decay of spectrometer sensitivity to $^{13}CO_2$ and ^{13}CO, as was argued at the beginning of this subsection.

Conclusions

The Shuttle environment was modeled in several situations, for which quantitative fluxes were predicted. All of them were compared to the EOIM-III mass spectrometer measurements, and the agreement was generally very satisfactory.

The first two cases simulated the backflow of outgassed species and thruster effluents into the Shuttle bay, during the quiescent period and VRCS operation, respectively. Because the absolute values of fluxes to be compared were dependent on the spectrometer sensitivity to the observed molecules, accuracy could not be expected to exceed approximately a factor of 2. An agreement was effectively found in that range. This essentially validated the DSMC model of transport through collisions.

The last simulation dealt with gasdynamics in the Shuttle bay, which is predominantly ruled by reflections on walls and erosion by AO. Considering ratios of the same mass signal in two different configurations (tilt-down/tilt-up or baffle on/baffle off) led to the expectation of improved accuracy. Agreement was obtained within 25% for AO fluxes. It was only within 70% for fluxes of erosion products, and simulations performed for several different accommodation coefficients and rates of Kapton erosion by AO exhibit a better agreement for high accommodation and small erosion efficiency at low AO energy.

It could be interesting to further validate the numerical model used in the study by applying it to other experimental studies. Quartz crystal microbalance experiments may have the advantage of producing quantitative deposit weight data. The major experimental uncertainties, however, would lie in the knowledge of condensable contaminant outgassing, as well as the sticking coefficient on crystal, more than in transport mechanisms that were the main phenomena tested in the model here.

Acknowledgments

All the people from Los Alamos National Laboratory, the U.S. Air Force, Lockheed, and especially NASA Johnson Space Center, who worked on EOIM-III flight experiment, are gratefully acknowledged for furnishing us the flight data.

References

[1]Koontz, S. L., Leger, L. J., Rickman, S. L., Hakes, C. L., Bui, D. T., Hunton, D. E., and Cross, J. B., "Oxygen Interaction with Materials III: Mission and Induced Environments," *Journal of Spacecraft and Rockets*, Vol. 32, No, 3, 1995, pp. 475–482.

[2]Koontz, S. L., Leger, L. J., Visentine, J. T., Hunton, D. E., Cross, J. B., and Hakes, C. L., "EOIM-III Mass Spectrometry and Polymer Chemistry: STS 46, July–August 1992," *Journal of Spacecraft and Rockets*, Vol. 32, No, 3, 1995, pp. 483–495.

[3]Cross, J. B., Koontz, S. L., and Hunton, D. E., "Flight Mass-Spectrometer Calibration in a High-Velocity Atomic-Oxygen Beam," *Journal of Spacecraft and Rockets*, Vol. 32, No, 3, 1995, pp. 496–501.

[4]Bird, G. A., *Molecular Gas Dynamics*, 1st ed., Oxford Univ. Press, Oxford, 1976, pp. 118–132.

[5]Bird, G. A., *Molecular Gas Dynamics and the Direct Simulation of Gas Flows*, 1st ed., Clarendon, Oxford, 1994, pp. 148–182.

[6]Bourdon, A., and Roussel, J.-F., "Contamination Transport: Numerical Simulation and Comparison to In-flight Experiment," *Optical Systems Contamination and Degradation*, edited by P. T. Chen, W. E. McClintock, and G. T. Rottman, Vol. 3427, Proceedings of SPIE, SPIE–The International Society for Optical Engineering, Bellingham, WA, 1998, pp. 324–334.

[7]Roussel, J.-F., "Spacecraft Plasma Environment and Contamination Simulation Code: Description and First Tests," *Journal of Spacecraft and Rockets*, Vol. 35, No, 2, 1998, pp. 205–211.

[8]Koontz, S. L., Cross, J. B., Hunton, D. E., and Lan, E., "Characterization and Calibration of the EOIM-III Flight Mass Spectrometer in a High Velocity Oxygen Atom Beam," *Materials Degradation in Low Earth Orbit*, edited by V. Srinivasan and B. A. Banks, Minerals, Metals, and Materials Society, Warrendale, PA, 1990, pp. 155–174.

[9]Scialdone, J. J., "An Estimate of the Outgassing of Space Payloads and its Gaseous Influence on the Environment," *Journal of Spacecraft and Rockets*, Vol. 23, No, 4, 1986, pp. 373–378.

[10]Scott, H. E., Frazine, D. F., and Lund, E. G., "Bipropellant Engine Plume Study," *Proceedings of the USAF/NASA International Spacecraft Contamination Conference*, NASA CP-2039, 1978, pp. 682–740.

[11]Bourdon, A., "Etude de l'Environnement Induit de la Navette: Exploitation des Données en Vol EOIM-III et Comparaison à une Simulation Numérique," Ph.D. Dissertation, ONERA/Space Environment Dept., Ecole Nationale Supérieure de l'Aéronautique et de l'Espace, Toulouse, France, Dec. 1998.

[12]Balakrishnan, N., Kharchenko, V., and Dalgarno, A., "Slowing of Energetic $O(^3P)$ Atoms in Collisions with N^2," *Journal of Geophysical Research*, Vol. 103, No, A10, 1998, pp. 23,393–23,398.

[13]Nocilla, S., "On the Interaction Between Stream and Body in Free-Molecule Flow," *Proceedings of the Rarefied Gas Dynamics Second International Symposium*, Academic, New York, 1961, pp. 169–208.

[14]Collins, F. G., and Knox, E. C., "Parameters of Nocilla Gas/Surface Interaction Model from Measured Accommodation Coefficients," *AIAA Journal*, Vol. 32, No, 4, 1994, pp. 765–773.

[15]Caledonia, G. E., Krech, R. H., and Oakes, D. B., "Laboratory Studies of Fast Oxygen Atom Interactions with Materials," *Proceedings of the Sixth International Symposium on Materials in a Space Environment*, ESA SP-368, European Space Research and Technology Center, Noordwijk, The Netherlands, 1994, pp. 285–290.

[16]Krech, R. H., Gauthier, M. J., and Caledonia, G. E., "High Velocity Atomic Oxygen/Surface Accommodation Studies," *Journal of Spacecraft and Rockets*, Vol. 30, No, 4, 1993, pp. 509–513.

[17]Cazaubon, B., Paillous, A., Siffre, J., and Thomas, R., "Five-Electron-Volt Atomic Oxygen Pulsed-Beam Characterization by Quadrupolar Spectrometry," *Journal of Spacecraft and Rockets*, Vol. 33, No, 6, 1996, pp. 870–876.

[18]Koontz, S. L., Albyn, K., and Leger, L. J., "Atomic Oxygen Testing with Thermal Atom Systems: A Critical Evaluation," *Journal of Spacecraft and Rockets*, Vol. 28, No, 3, 1991, pp. 315–323.

I. D. Boyd
Associate Editor